Scientific Research Publishing

Open Journal of Geology, 2022, 12, 1013-1031
https://www.scirp.org/journal/ojg
ISSN Online: 2161-7589
ISSN Print: 2161-7570

Implication of Paleoproterozoic Basalt Fertility Related to Mantle Plume Activity in Nassara Gold Mineralization (Burkina Faso, West Africa)

Pascal Ouiya[1,2*], Adama Ouédraogo Yaméogo[2,3], Hermann Ilboudo[2], Séta Naba[2]

[1]Ecole Normale Supérieure (ENS), Institut Sciences et Technologies (IST), Ouagadougou, Burkina Faso
[2]Laboratoire Géosciences et Environnement (LaGe), département des Sciences de la Terre, Ouagadougou, Burkina Faso
[3]Université Norbert ZONGO (UNZ), Koudougou, Burkina Faso
Email: *pascal.ouiya@gmail.com

How to cite this paper: Ouiya, P., Yaméogo, A.O., Ilboudo, H. and Naba, S. (2022) Implication of Paleoproterozoic Basalt Fertility Related to Mantle Plume Activity in Nassara Gold Mineralization (Burkina Faso, West Africa). *Open Journal of Geology*, **12**, 1013-1031.
https://doi.org/10.4236/ojg.2022.1211048

Received: October 12, 2022
Accepted: November 27, 2022
Published: November 30, 2022

Abstract

The Birimian Nassara volcanic formations are located south of Gaoua in the southern part of the Boromo belt. Within these formations is the Nassara gold deposit where mineralization is hosted at the contact between basaltic volcanic rocks and sedimentary rocks. It is with the aim of understanding the geodynamic context of the basaltic rocks and the implication of their primary gold potential in the Nassara gold deposit that this work is carried out. To achieve our objectives, 28 samples of fresh basaltic rocks were geochemically analyzed for their major and trace element compositions. These analyses show that the Nassara basalts are Fe-rich tholeiitic basalts. Rare earth profiles (La/Sm_N = 0.75 - 1.50; La/Yb_N = 0.65 - 2.18) are fairly flat and without europium anomaly (Eu/Eu^* = 0.90 - 1.09), nor niobium. In the Zr/Nb vs. Nb/Th and Nb/Y vs. Zr/Y binary diagrams, the Fe-rich tholeiitic basalts of Nassara, as well as those of the Houndé and Boromo belts, are placed in the field of oceanic plateau basalts related to a mantle plume system. A gold fertility test carried out on these basalts was positive. As other studies have already shown, the genetic link between gold deposits and mantle plumes appears to be a general rule. The scenario for the Nassara gold deposit is that it is the source magma that was already more or less enriched in gold and other related elements on its way up. The remobilization of this gold would have occurred during the Eburnean orogeny with the help of metamorphic, hydrothermal and deformation phenomena to be redeposited at the level of shear zones with economic grades. Through this analysis, we show that the fertility of the initial lithologies is very important for the formation of economic size deposits in the proximal shear zones. Exploration work should now integrate this

dimension to define the best targets.

Keywords

Nassara Gold Deposit, Fe-Rich Basalt, Oceanic Plateau, Mantle Plume, Gold Fertility

1. Introduction

The formations of the Man/Leo Ridge are organized into the Archean domain in the east and the Paleoproterozoic domain in the west (**Figure 1**). The Paleoproterozoic formations of the Baoulé-mossi domain are known as the Birimian formations [1]. These formations were emplaced around 2.1 Ga and represented a period of significant crustal accretion during the Eburnian orogeny [2].

In terms of geochemistry, it is generally agreed that the birimian formations are rocks related to rocks related to bimodal volcanism [3]-[8]. This bimodal volcanism is characterized by rocks with tholeiitic affinity and rocks with calc-alkaline affinity. The magmatism of the Upper Birimian calc-alkaline formations is related to intra-oceanic subduction zones evolving into an active continental margin (Lambert Smith et al., 2016). However, the geodynamic context of basalt emplacement remains a matter of debate. A first group proposes an island arc context [8] [9] [10] [11] [12]. A second group proposes a mantle plume context [3] [4] and finally the last group proposes a mid-ocean wrinkle context [13].

In the Houndé belt, tholeiitic basalts are emplaced in an oceanic shelf context [14]. In the Boromo and Houndébelts, [8] showed emplacement in an island

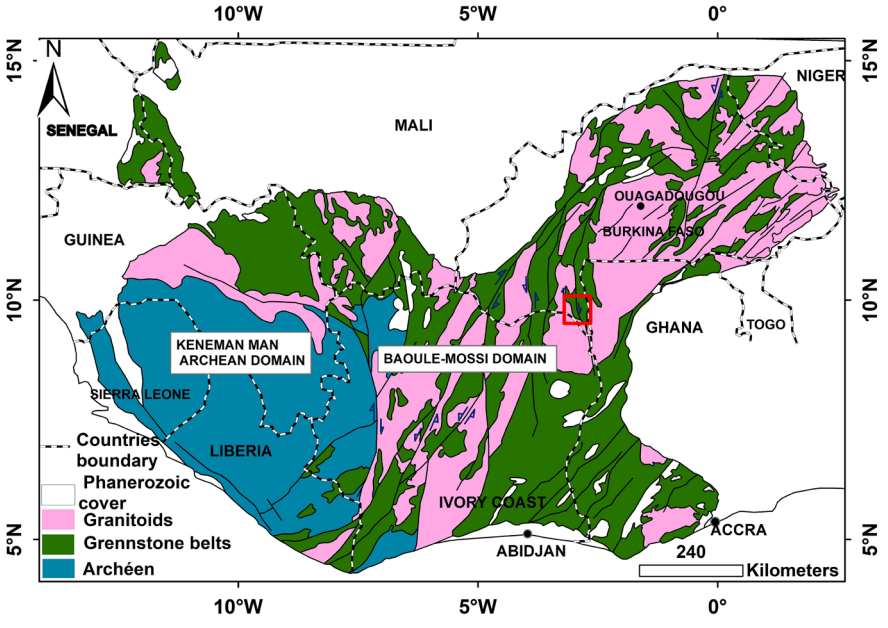

Figure 1. Lithostructural map of the Man/Léo shield showing the different formations and the main structures (modified from [18]).

arc context. In the Guiana Craton, [15] showed that the El Calao basalts were emplaced in an oceanic plateau context for a mantle plume source.

Most orogenic gold deposits in the Man/Léo Ridge and in particular in Burkina Faso are contained in greenstone belts (**Figure 2(a)**). Many works have recently shown that the source of primary gold orogenic is related to the emplacement of intrusions, pyrite-rich carbonaceous sedimentary rocks and basaltic rocks [14] [15] [16]. Radiometric ages obtained from orogenic gold dating in different West African deposits show that the primary gold was emplaced between 2200 and 2120 Ma [17] and correspond to the major period of accretion of the Birimian formations around 2.25 to 1.98 Ga [2]. This coincidence shows that it was during the metamorphic and hydrothermal processes of the Eburnian orogeny that the primary gold was remobilized. The Boromo greenstone belt is known for its gold and base metal potential. These include the Poura, Konkéra, Torkéra and Nassara gold deposits, the Perkoa zinc deposit, and the Diénéméra-Gongondy copper porphyry.

The Nassara gold deposit located south of this belt is the subject of this study. The aim is to characterize the geodynamic setting of the Nassara gold deposit basalts and their primary gold potential. This study will be based mainly on geochemical analysis data on total rock (major and trace). These data will also be compared to other data obtained during previous work in the West African craton.

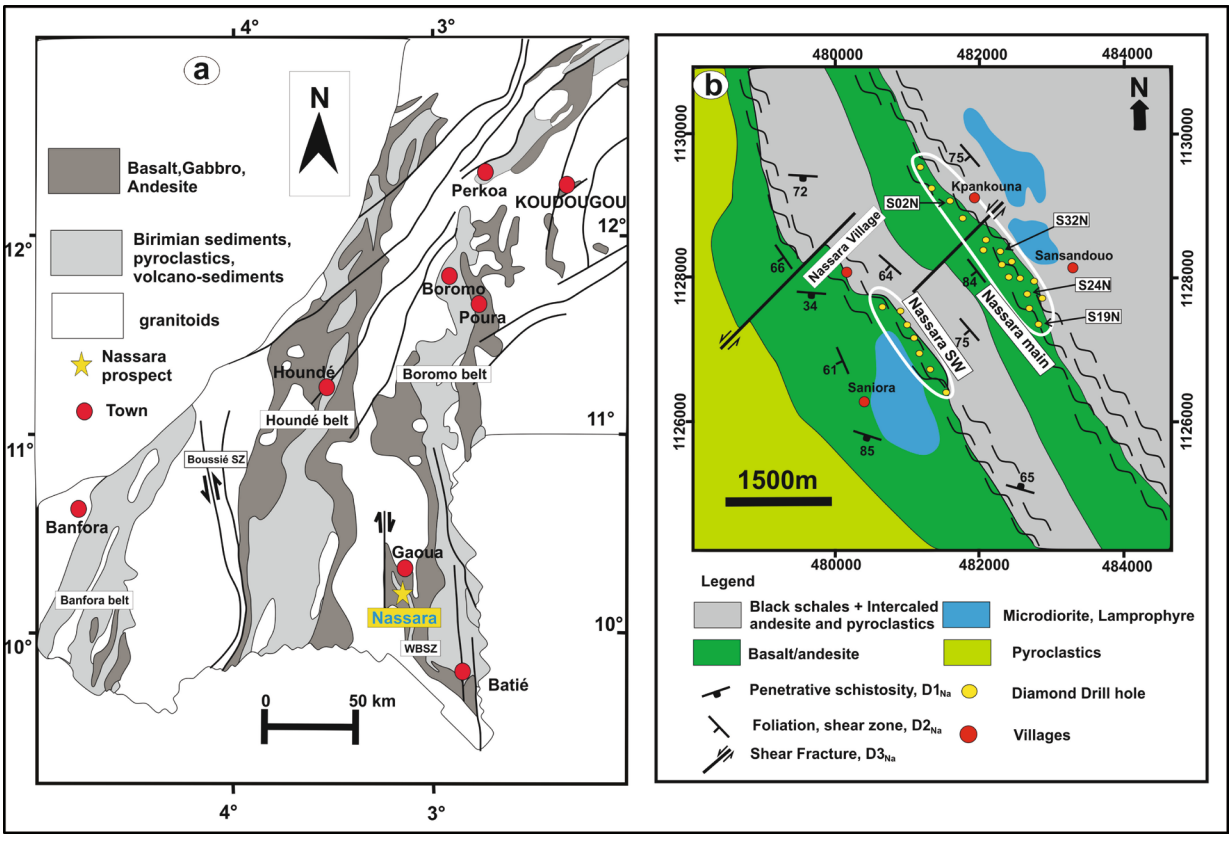

Figure 2. Regional geological setting of the study area: (a) Simplified geological map of the southwestern part of Burkina Faso (modified from [8]) (b) Geological map of the Nassara area with the positions of the core holes taken.

2. Regional Geological Setting

Like the entire Paleoproterozoic domain (Baoulé-Mossi domain) of the Man/Léo Ridge, in the Gaoua region, the Birimian formations are organized in greenstone belts formed essentially by a volcanic sequence and a volcano-sedimentary and sedimentary sequence representing the Birimian supergroup. At the limit of these greenstone belts are vast batholiths of tonalite, trondhjemite and granodiorite (TTG) which are syn-tectonic granitoids [19] [20]. The greenstone belts and batholiths (TTG) are later intruded by granitoids of various compositions, with calc-alkaline or alkaline affinity [18] [19] [21] [22] [23].

On the basis of lithostratigraphy, the Birimian supergroup consists of a lower birimian formed by ultrabasite, pillow lava basalt with tholeiitic affinity and andesites overlain by sediments. The upper birimian is dominated by sediments cut by basic to intermediate volcanic dykes with calc-alkaline affinity (dacite, rhyodacite, rhyolite). At its top is a thick detrital layer of sediment and carbonaceous rocks [5] [8] [24] [25] [26] [27] [28].

The Nassara gold prospect (**Figure 2(b)**) is located in the Boromo belt along the West Batié Shear Zone (WBSZ) south of Gaoua where the formations are essentially volcanic, volcanosedimentary and sedimentary rocks. The formations of the Nassara zone are essentially basalts, basaltic andesites, dacites, rhyodacites and granitoids. This ensemble is intersected by circumscribed intrusives of diorite and lamprophyre dykes [29]. These formations are affected by polyphase deformation throughout the Nassara Zone [29] [30].

3. Methodology

To carry out this work we collected core samples from different holes along the mineralized corridor. After microscopic observations, the freshest samples were taken for geochemical analysis. Samples were also collected from outcrops in the shear corridor. A set of twenty-eight (28) samples were selected, crushed for some and ground into a fine powder at the Geosciences and Environment Laboratory of Toulouse (GET). The powders of the different samples were conditioned in vials and labeled then sent for analysis. Major and trace elements were mainly measured by ICP-MS and ICP-AES at ALS (Spain). For more information you can visit the following website: https://www.alsglobal.com/.

4. Results

The Nassara basalts contain between 47.2 and 50.5 wt% SiO_2, between 10.1 and 16.2 wt% Fe_2O_3, between 4.6 and 12.3 wt% MgO and 0.42 to 1.25 wt% TiO_2. The different rock trends are recorded in **Table 1**. In the SiO_2 Vs Zr/TiO_2 * 0.0001 binary diagram of [31], the rocks confirm their basaltic nature (**Figure 3**).

Magmatic affinities tested for the Nassara basalts in the AFM diagram of [32] show that they have a highly iron-rich tholeiitic affinity (**Figure 4**), which is similar to the basalts of the Houndé and Boromo belts [8] [14]. Based on trace elements, we calculated Zr/Y ratios (**Table 1**). According to the work of Barrett

Table 1. Representative major (wt%) and trace (ppm) element compositions for the Nassara basalts rocks.

SAMPLE	Ba1	Ba2	Ba3	Ba4	Ba5	Ba6	Ba7	Ba8	Ba9	Ba10	Ba11	Ba12	Ba13	Ba14
Major elements (wt%)														
SiO_2	50	49.9	49.8	49.7	44	49.7	50.1	50.5	49.3	50.4	45.2	49.7	47.8	49.9
Al_2O_3	14	14.6	14.35	12.9	12.6	13.3	13.3	8.21	14.2	8.41	10.8	11.9	18.5	14.2
Fe_2O_3	13	13.4	14.55	15.2	12.9	15.2	15.3	10.8	14.5	10.9	10.3	11.9	10.6	13.8
CaO	11	10.1	10.75	10	8.42	6.63	6.55	14.3	10.8	14	9.53	10.5	13.4	10.4
MgO	7.8	7.37	5.32	6.25	4.23	6.34	6.4	12.3	6.05	12.3	8.04	9.24	5.54	6.58
Na_2O	2	2.25	1.3	2.08	0.56	3.45	3.42	1.3	1.87	1.39	1.26	1.84	1.38	2.76
K_2O	0.3	0.11	0.01	0.2	1.97	0.04	0.03	0.34	0.19	0.31	0.77	1.23	0.14	0.19
TiO_2	0.8	0.98	1.2	1.06	1.11	1.18	1.22	0.42	0.94	0.42	0.5	0.63	0.63	0.88
MnO	0.2	0.19	0.2	0.22	0.16	0.21	0.21	0.21	0.21	0.21	0.16	0.2	0.16	0.22
P_2O_5	0.1	0.09	0.17	0.1	0.11	0.11	0.12	0.08	0.08	0.08	0.12	0.17	0.05	0.07
LOI	2.7	2.85	3.81	2.72	14.2	3.87	3.82	2.23	2.35	2.23	12.8	3.32	2.17	1.17
total	102	101	101.5	100.5	100.3	100.2	100.6	100.9	100.6	100.7	99.6	100.7	100.4	100.2
Traces elements (ppm)														
Ba	107	27.6	12.8	110	170	30	30	280	30	270	160	380	30	40
Ce	7.8	8.7	14.7	10.8	13.2	8.4	8.6	6.4	9.7	6.2	9.1	11.2	4.9	6.8
Cr	540	280	190	110	70	100	100	720	110	730	340	390	200	180
Cs	0.5	0.27	0.14	0.2	2.7	0.4	0.4	0.3	0	0.3	2.6	0.5	0.2	0.2
Dy	3.2	3.81	5.47	4.55	4.3	4.83	4.92	1.94	3.94	1.94	2.04	2.6	2.47	3.43
Er	2.1	2.49	4.11	2.92	2.73	3.38	3.33	1.22	2.57	1.31	1.36	1.61	1.69	2.27
Eu	0.7	0.8	1.3	0.97	0.93	0.93	1.03	0.51	0.86	0.49	0.54	0.66	0.6	0.68
Ga	15	16.1	19	16	16	16	16	9	16	9	11	12	15	15
Gd	2.7	3.2	4.72	3.57	3.52	3.66	3.77	1.75	3.02	1.78	1.98	2.31	2	2.73
Hf	1.6	1.9	2.8	2	2	2	2	0	2	0	0	1	0	1
Ho	0.7	0.8	1.24	0.95	0.93	1.06	1.09	0.4	0.83	0.42	0.42	0.55	0.53	0.73
La	3	3.2	5.8	4.2	5.1	3.2	3.2	2.7	3.6	2.8	3.8	4.8	1.8	2.5
Lu	0.3	0.39	0.6	0.42	0.39	0.49	0.47	0.17	0.35	0.17	0.18	0.22	0.25	0.33
Nb	2.5	2.4	5.9	3										
Nd	5.7	6.8	10.2	8.4	9.6	7.4	7.3	4.8	7.1	4.9	6.1	7.4	4.2	5.8
Pr	1.2	1.36	2.14	1.62	1.89	1.36	1.37	0.94	1.49	0.95	1.27	1.57	0.76	1.07
Rb	7.3	2.7	0.2	4.5	48.6	1	1	4.6	3.3	4.6	30.8	24.6	2.7	2.7
Sm	1.9	2.26	3.37	2.7	2.8	2.6	2.5	1.4	2.4	1.3	1.7	2	1.4	1.9
Sr	143	185	194	130	100	230	230	380	170	400	280	310	150	80
Tb	0.5	0.56	0.82	0.64	0.63	0.69	0.7	0.29	0.58	0.3	0.32	0.37	0.36	0.5
Th	0.3	0.22	0.43	0.6	0.6	0.4	0.3	0.4	0.4	0.4	0.5	0.7	0.2	0.3
Tl	0.5	0.5	0.5	0.66	0.67	0.72	0.72	0.26	0.58	0.27	0.31	0.37	0.38	0.52
Tm	0.3	0.35	0.61	0.43	0.41	0.49	0.48	0.17	0.36	0.18	0.18	0.24	0.25	0.34
U	0.2	0.07	0.14	0.11	0.22	0.09	0.09	0.19	0.11	0.18	0.27	0.34	0.07	0.07

Continued

V	322	363	297	363	325	368	361	248	327	247	240	269	232	311
Y	19	22.4	34.6	24	22.5	25.2	25.5	10.1	19.8	10.2	10.8	13	13.5	18.4
Yb	2.2	2.48	3.91	2.7	2.6	3.1	3.1	1.2	2.4	1.2	1.2	1.5	1.6	2.2
Zr	51	56	91	69.2	71.7	60.4	58.4	27.3	64.5	32.1	31.7	35	33.1	44.7
Co	49	48	44	54.8	48.6	51.6	52.6	49.7	54.5	50.5	41.6	44.5	42.7	51.9
Cu	183	150	157	180	150	130	120	50	150	40	120	100	110	140
Ni	162	146	85	85	59	78	71	81	89	81	55	59	105	101
Zr/Y	2.68	2.5	2.63	2.88	3.18	2.39	2.29	2.7	3.25	3.14	2.93	2.69	2.45	2.42
Zr/Nb	20.4	23.33	15.42	23.06										
Nb/Th	8.33	10.90	13.72	5										
Nb/Y	0.13	0.10	0.17	0.12										
Eu/Eu*	0.94	0.91	0.99	0.95	0.95	0.90	0.92	1.02	0.99	0.97	0.98	0.90	0.94	1.09
(La/Yb)N	0.93	0.88	1.01	0.97	1.06	1.33	0.70	0.70	1.53	1.02	1.59	2.16	2.18	0.77
(La/Sm)N	0.99	0.89	1.08	0.82	0.97	1.14	0.77	0.80	1.21	0.94	1.35	1.40	1.50	0.81
Au	-	-	-	3	44	0	0	0	0	2	5	0	1	0

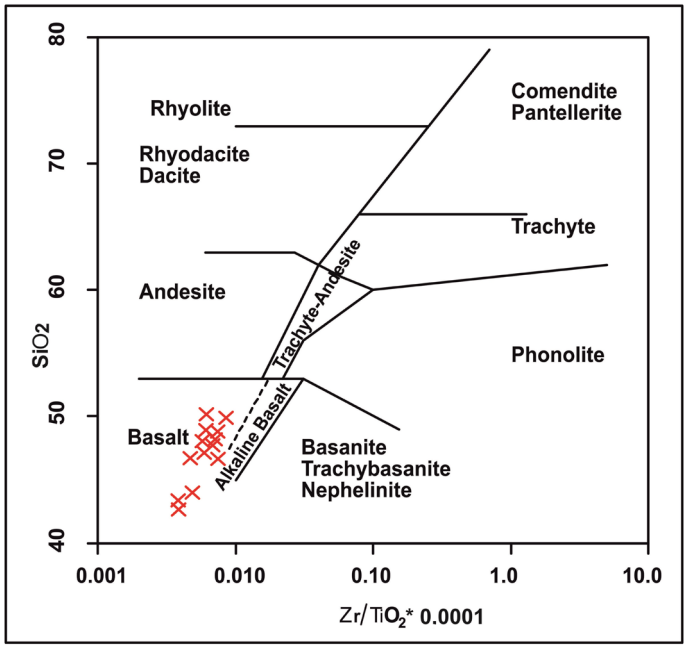

Figure 3. Positions of the Nassara volcanic rocks (red cross) on the diagram SiO2 Vs. $(Zr/TiO_2) \times 0.0001$ [31].

and maclean (1999), ratios < 4 correspond to a tholeiitic affinity, ratios > 7 show a calc-alkaline affinity. Ratios between these two values correspond to a transition lineage. For the Nassara basalts, the values are between 2.03 and 2.67 confirming their tholeiitic affinity. This character is confirmed in the diagram of [33], where the Nassara basalts like other Paleoproterozoic basalts of the West African craton [8] [13] are placed in the tholeiitic field (Figure 5). The Nassara basalts are highly Fe-rich tholeiites.

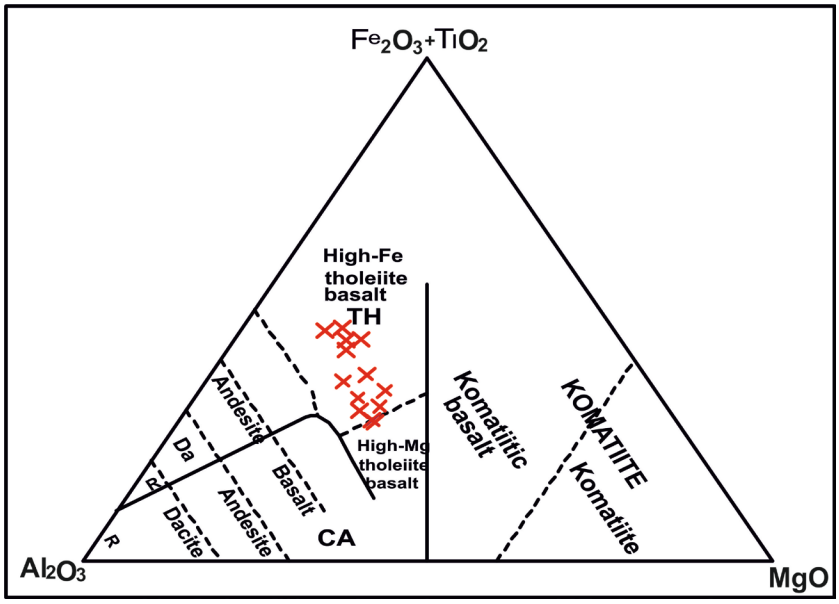

Figure 4. Positions of the Nassara volcanic rocks (red cross) on the discrimination diagram [32]. Labels: TH, tholeiite field; Ca, calc-alkaline field with R, rhyolite, Da, dacite.

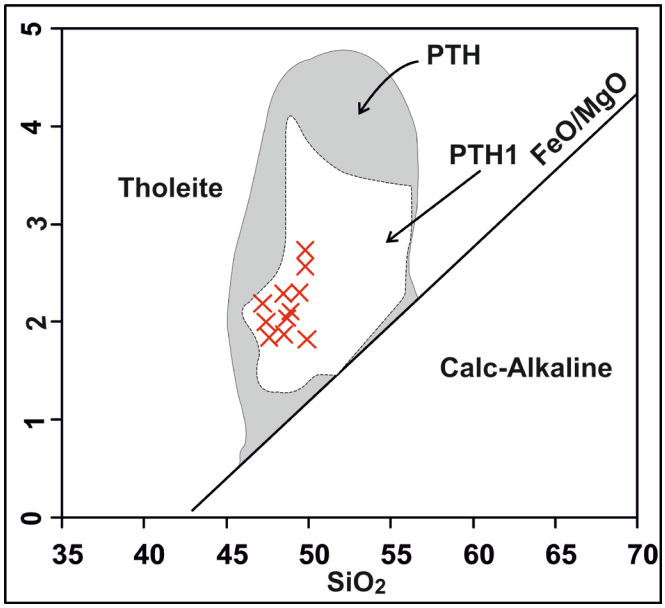

Figure 5. Positions of the Nassara volcanic rocks (red cross) on the Feo/MgO Vs. SiO_2 diagram [33] showing also the field of the paleoproterozoic tholeiitic series (PTH, PTH1) of the West African Craton after [13].

In the diagram of [34], the rare earth spectra (**Figure 6**) normalized to chondrite (La/Sm_N = 0.75 - 1.50; La/Yb_N = 0.65 - 2.18) are flat with no significant europium anomaly (Eu/Eu* = 0.90 - 1.09) suggesting little or no plagioclase fractionation. By these characters, the Nassara basalts show similarities to those of the West African craton oceanic shelves [13] [14], to those of the Pacific oceanic plateaus [35] (**Figure 7**). In the trace element spider diagram [36] normalized to the early mantle (**Figure 8**), a flat spectrum is observed for high field strength

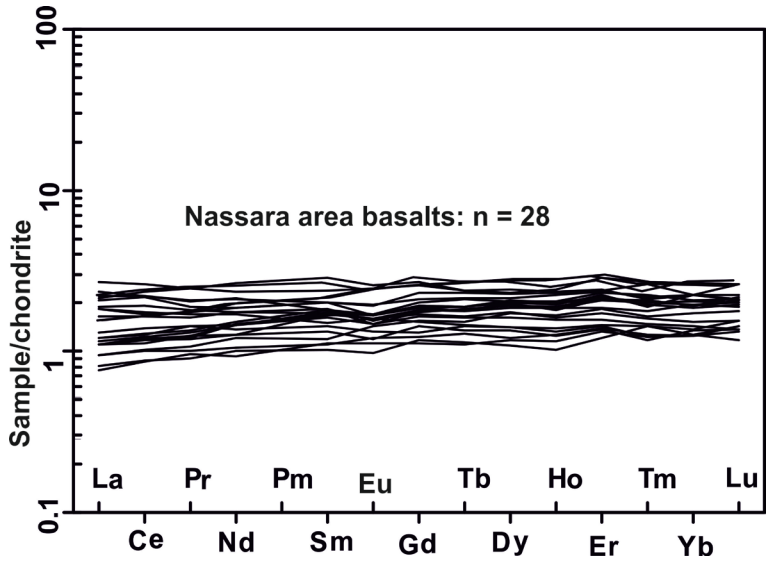

Figure 6. Chondrite normalized rare earth element diagram for the Nassara basalts [34].

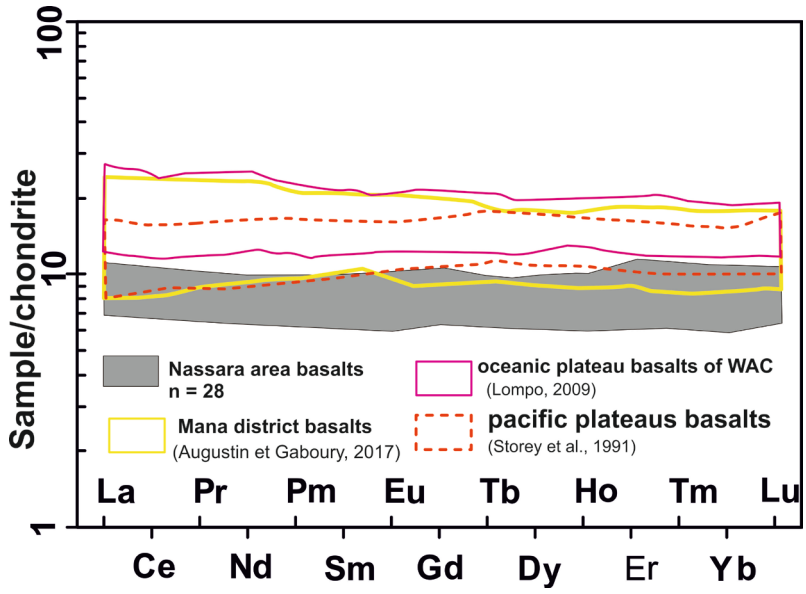

Figure 7. Comparison with oceanic plateau basalts of the WAC [13] [14], and modern Pacific Plateau basalt fields [35].

elements (HFSE) except for Ti where a negative anomaly is observed; the absence of a niobium anomaly suggests that there is no crustal contamination. The slight negative anomaly in titanium reflects a slight fractionation of the oxides. The variation of the Sr anomaly, sometimes positive and sometimes negative, the negative Rb anomaly, and the negative K anomaly suggest a slight hydrothermal alteration.

5. Discussion

The geodynamic context of the West African Craton (WAC) basaltic formations is defined by two groups of authors. A first group of authors [6] [8] [9] [10] [11]

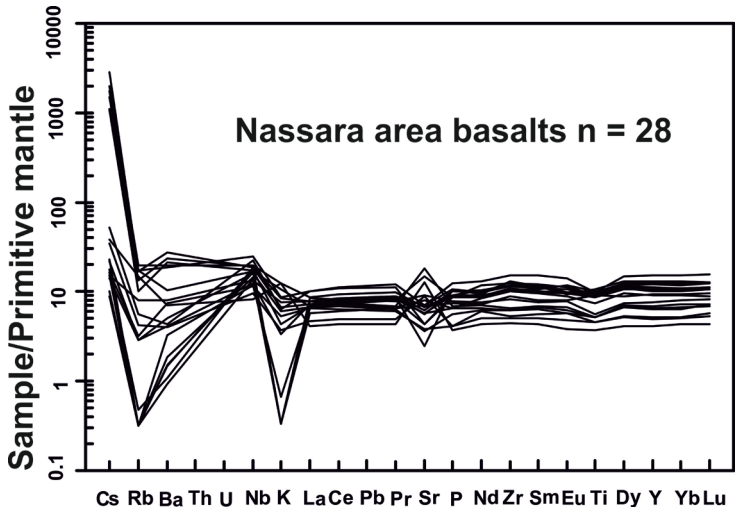

Figure 8. Spidergram of trace elements normalized to the primitive mantle for the Nassara basalts [36].

[12] propose that the WAC basalts formed in a mid-ocean rift context or in an island arc context. The second group of authors proposes an oceanic shelf context with mantle plume activity [3] [4] [13] [14] [37] [38]. [13] defined three types of tholeiites for the WAC formations ranging from PTH1 to PTH3. For the geodynamic setting, he proposes an oceanic basin formed by subsidence.

In what follows, the geochemical characteristics of the Nassara basalts compared to similar materials in the West African craton and worldwide will be discussed in turn. These include the geodynamic context of emplacement, the source of the magma, possible crustal contamination of the magma, and their possible implication as the source of the primary gold.

5.1. Implications for Tectonic Setting

According to [39], island arc basalts have a niobiom (Nb) content of less than 2 ppm. and thus [40] discriminated mid-ocean rift basalts (MORB) with an Nb content < 3 ppm and ocean plateau basalts (OPB) with an Nb content > 5 ppm. Another boundary between the two types of basalts [40] is based on the La/Nb ratio. MORBs have a La/Nb ratio > 1.4 and La/Nb values < 1.4 are unique to oceanic shelf basalts. [15] also relied on niobium content to discriminate Paleoproterozoic basalts from El calao as ocean plateau basalts.

Analytical data for the Nassara basalts show that the niobiom content is between 2 - 5.9, and La/Nb ratios between 0.9 and 1.4 are also less than or equal to 1.4. The flat rare-earth spectra without significant europium anomaly show low fractionations (La/SmCN = 0.75 - 1.14; La/YbCN = 0.65 - 1.22). All these characteristics allow us to say that the Nassara basalts were emplaced in an oceanic plateau context.

5.2. Mantle Source

A discriminating argument to show the mantle origin of the magmas is the use

of Nb/Th-Zr/Nb and Zr/Y-Nb/Y diagrams, because these elements are incompatible in the mantle. The position of our data in the Nb/Th-Zr/Nb and Zr/Y-Nb/Y diagrams [41] [42] (**Figure 9** & **Figure 10**) shows that they are mantle-sourced

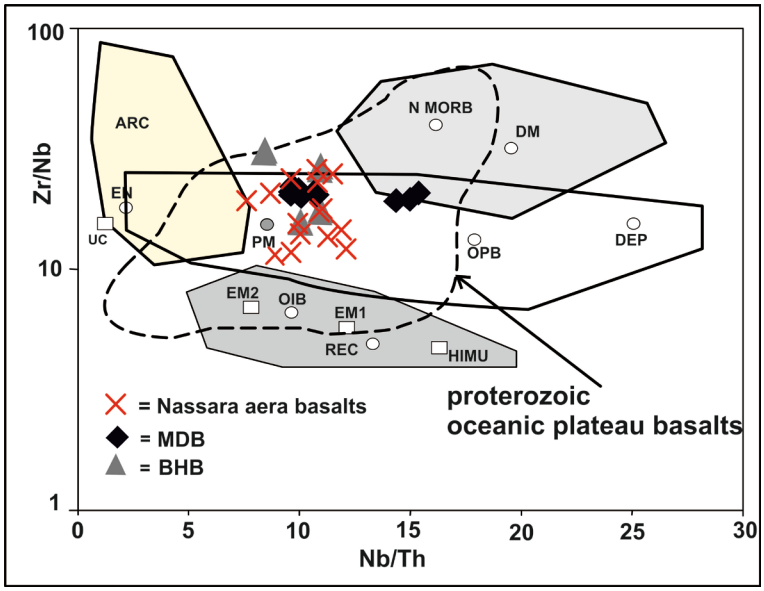

Figure 9. Binary Zr/Nb vs. Nb/Th diagram for the Nassara area basalts. Composition is compared with those of basalt of western Burkina Faso [8]: BHB; [14]: MDB). BHB: Boromo Houndé basalt; MDB: Mana district basalt ARC: arc related basalts; N-MORB: Normal mid ocean ridge basalt; OIB: oceanic island basalt. DM: shallow depleted mantle; EN: enriched component; PM: primitive mantle; REC: recycling component; UC: upper continental crust; DEP: depleted plume component; HIMU: high μ(U/Pb) source; EM1 and EM2: enriched mantle sources (modified after [41] [42]). Proterozoic plateau oceanic basalts are from [41].

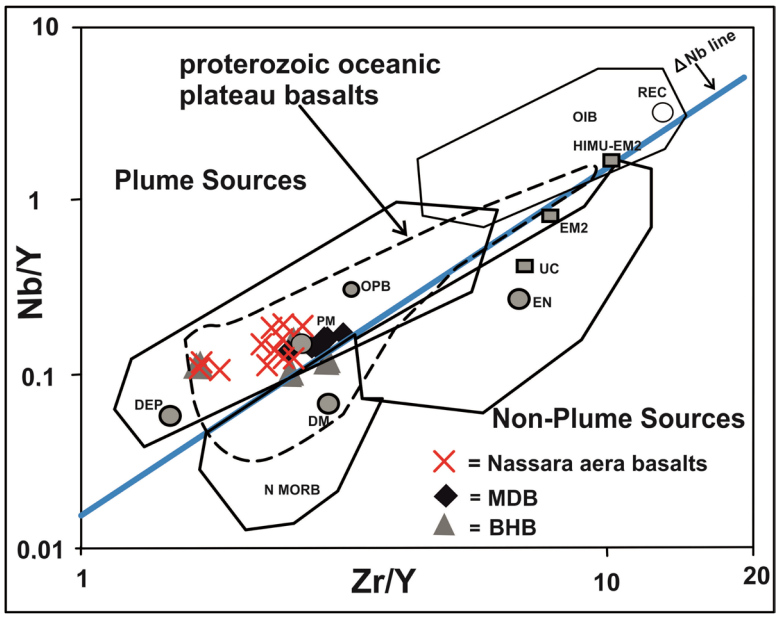

Figure 10. Plot of Nb/Y vs. Zr/Y for the Nassara area basalt. See **Figure 9** for symbols and other information.

magma that would have been emplaced in an oceanic plateau environment as a mantle plume. In the WAC, similar emplacement contexts in mantle-sourced oceanic shelf environments have already been proposed for tholeiitic basalts [3] [4] [13].

Work by [42] has also shown that relationships between elements such as Zr-Y-Nb-Th provide useful geochemical fingerprints for distinguishing mantle plume head and tail. For the Nassara case, this may well be a mantle plume head source for the Nassara basalts. In addition, the source of the parental magma can be distinguished on the basis of MgO content [43]. For example, they define for the tail of the plume magnesium-rich komatiitic rocks, for the central part of the plume magnesian komatiites and for the head of the plume weakly magnesian komatiites.

On this basis, we can say that the composition of the Fe-rich Nassara tholeiitic basalts corresponds to a plume head origin probably from its peripheral part. Another alternative proposed as sources of the Paleoproterozoic iron-rich tholeiites named PHT1 and PHT2 [13] is that of partial mantle melting at depth.

5.3. Crustal Contamination

Geochemical data from the Nassara Zone basalts do not show a negative Nb anomaly, characteristic of crustal contamination. This observation has already been made by a number of previous works based on isotopic data, suggesting the juvenile character of the Paleoproterozoic crust of the West African craton [3] [4] [10] [20] [25] [27] [36]. Furthermore, the La/Sm_N ratio of 0.75 to 1.14 (<1.5) of the Nassara Zone basalts supports the idea of a mantle magma that has not undergone contamination [44].

5.4. Implications for Gold Sources

The Nassara basalts, which were emplaced in an oceanic plateau setting as a mantle plume, are believed to be fertile in gold from the source magma that was more or less enriched in gold and other related elements on its way up. This was confirmed by the fertility test performed on samples not affected by hydrothermalism taken outside the mineralized corridor. Indeed, it is shown that most large orogenic gold deposits and large gold provinces are related to mantle plume activity that generally favors lithospheric growth in an active continental margin setting [14] [15] [45] [46] [47] [48] [49].

This predisposition is probably due to the fact that the source of the mantle plumes can originate from the core-mantle boundary and thus transport the gold-enriched material upward [50]. These same authors believe that hot mantle activity in contact with the crust causes devolatilization and melting of the crust which is a precursor for large orogenic gold deposits.

The Nassara gold deposit is thought to be due to remobilization of primary gold from basalts by metamorphic and hydrothermal processes and its deposition in low pressure zones created by contemporary tectonics during the Ebur-

nian orogeny. This interpretation is in agreement with the work of [48] and [51] who shows that orogenic deposits are located in shear zones as a result of metamorphic processes. In relation to this remobilization issue, [52] estimated that 19 km^3 of tholeiitic basalts with 1 ppb of primary mineralization is required to form a 1Moz gold deposit.

In the West African Craton and in particular in the Man/Leo Ridge, recent work has shown by the Re-Os method that orogenic-type gold mineralization contained in the shear zones is between the period of 2150 Ma and 2085 Ma ± 71 Ma [17]. These same authors dated the gold mineralization at Nassara to 2094 ± 58 Ma. This age could be interpreted as the age of the metamorphic and hydrothermal processes that led to the remobilization of the primary gold and the emplacement of the Nassara gold deposit. Numerous works [29] [53] among others) have shown that large gold deposits developed at the contact between tholeiitic basalts and sedimentary rocks. The contact zones are indeed zones of weakness that are borrowed by the transcurrent shear that creates the dilatant structures able to channel the hydrothermal fluids that have circulated in the fertile basalts.

6. Conclusions

Major and trace element geochemical data allowed us to characterize the Nassara basalts as iron-rich tholeiitic basalts. They are also marked by fairly flat profiles through the rare earth elements normalized to chondrite and through the High field strength elements (HFSE) of trace elements normalized to the primitive mantle. The Zr/Nb vs. Nb/Th and Nb/Y vs. Zr/Y binary diagrams show that the Nassara Zone basalts were emplaced in an oceanic shelf setting emanating from a mantle plume. These basalts are the primary source of mineralization for the Nassara gold deposit. This gold was remobilized during metamorphic and hydrothermal processes and redeposited in shear zones.

This study shows that it is important to perform a rock fertility test in a mining exploration area to have the best chance of success.

Acknowledgements

This work is a part of the PhD thesis work that I defended in 2019 at Joseph KI ZERBO University. The authors want to thank the mining company B2Gold, through its chief geologist Mr. NARE Athanase for allowing us to sample the different rocks for the analyses. The WAXI-2 project funded the field work and geochemical analyses. The Institute of Research for Development (IRD) for its logistic support.

Conflicts of Interest

The authors declare that there is no conflict of interest with this paper.

References

[1] Bessoles, B. (1977) Géologie de l'Afrique. Le craton ouest-africain. Mémoires

BRGM, Paris, 88.

[2] Allibone, A.H., Campbell, M.T., Harrist, T., Etheridge, M., Munroe, S., Byrned, D., Amanor, J. and Gyapong, W. (2002) Structural Controls on Gold Mineralization at the Ashanti Gold Deposit, Obuasi, Ghana. Society of Economic Geology, Special Publication 9, 65-93. https://doi.org/10.5382/SP.09.04

[3] Abouchami, W., Boher, M., Michard, A. and Albarède, F. (1990) A Major 2.1 Ga Event of Mafic Magmatism in West Africa: An Early Stage of Crustal Accretion. *Journal of Geophysical Research*, **95**, 17605-17629. https://doi.org/10.1029/JB095iB11p17605

[4] Boher, M., Abouchamy, W., Michard, A., Albarede, F. and Arndt, N.T. (1992) Crustal Growth in West Africa at 2.1 Ga. *Journal of Geophysical Research*: *Solid Earth*, **97**, 345-369. https://doi.org/10.1029/91JB01640

[5] Vidal, M., Delor, C., Pouclet, A., Siméon, Y. and Alric, G. (1996) Evolution géodynamique de l'Afrique de l'Ouest entre 2.2 et 2 Ga: Le style "archéen" des ceintures vertes et des ensembles sédimentaires birimiens du nord-est de la Côte-d'Ivoire. *Bulletin de la Société Géologique de France*, **167**, 307-319.

[6] Béziat, D., Bourges, F., Débat, P., Lompo, M., Martin, F. and Tollon, F. (2000) A Paleoproterozoic Ultramafic-Mafic Assemblage and Associated Volcanic Activity in the West African Craton. *Precambrian Research*, **10**, 25-47. https://doi.org/10.1016/S0301-9268(99)00085-6

[7] Wenmenga, U. and Affaton, P. (2003) Les anomalies geochimiques (Pb-Zn-Cu) du district métallogénique de la région de Gaoua, ceinture Birimienne de Poura, Burkina Faso. *Journal of Mining and Geology*, **39**, 29-38. https://doi.org/10.4314/jmg.v39i1.18788

[8] Baratoux, L., Metelka, V., Naba, S., Jessell, M.W., Grégoire, M. and Ganne, J. (2011) Juvenile Paleoproterozoic Crust Evolution during the Eburnean Orogeny (~2.2-2.0 Ga), Western Burkina-Faso. *Precambrian Research*, **191**, 18-45. https://doi.org/10.1016/j.precamres.2011.08.010

[9] Zonou, S., Karche, J.P., Lapierre, H., Lemoine, S., Rossy, M. and Roques, M. (1985) Volcanismes tholéiitique et calco-alcalin dans les formations du Birrimien supérieur de Bouroum (N.E. Du Burkina-Faso). *Comptes rendus de l'Académie des Sciences Paris*, **301**.

[10] Ama Salah, J., Liégeois, P. and Pouclet, A. (1996) Evolution d'un arc insulaire océanique birimien précoce au Liptako nigérien (Sirba): Géochronologie et géochimie. *Journal of African Earth Science*, **22**, 235-254. https://doi.org/10.1016/0899-5362(96)00016-4

[11] Eglinger, A., Thébaud, N., Zeh, A., Davis, J., Miller, J., Parra-avila, L.A. and Belousova, E. (2017) New Insights into the Crustal Growth of the Paleoproterozoic Margin of the Archean Kéména-Man Domain , West African Craton (Guinea): Implications for Gold Mineral System. *Precambrian Research*, **292**, 258-289. https://doi.org/10.1016/j.precamres.2016.11.012

[12] Wane, O., Liégeois, J., Thébaud, N., Miller, J., Metelka, V. and Jessell, M. (2018) The Onset of the Eburnean Collision with the Kenema-Man Craton Evidenced by Plutonic and Volcano Sedimentary Rock Record of the Masssigui Region, Southern Mali. *Precambrian Research*, **305**, 444-478. https://doi.org/10.1016/j.precamres.2017.11.008

[13] Lompo, M. (2009) A Model of Subsidence of an Oceanic Plateau Magmatic Rocks in the MaleonShield of the West African Craton Geodynamic Evolution of the 2.25-2.0 Ga Paleoproterozoic. In: Reddy, S.M., Mazumder, R., Evans, D.A.D. and Collins,

A.S., Eds., *Paleoproterozoic Supercontinents and Global Evolution*, Geological Society, London, 231-254. https://doi.org/10.1144/SP323.11

[14] Augustin, J. and Gaboury, D. (2017) Paleoproterozoic Plume-Related Basaltic Rocks in the Mana Gold District in Western Burkina Faso, West Africa: Implications for Exploration and the Source of Gold in Orogenic Deposits. *Journal of African Earth Sciences*, **129**, 17-30. https://doi.org/10.1016/j.jafrearsci.2016.12.007

[15] Velasquez, G., Beziat, D., Salvi, S., Tosiani, T. and Debat, P. (2011) First Occurrence of Paleoproterozoic Oceanic Plateau in the Guiana Shield: The Gold-Bearing El Callao Formation, Venezuela. *Precambrian Research*, **186**, 181-192. https://doi.org/10.1016/j.precamres.2011.01.016

[16] Large, R.R., Maslennikov, V., Robert, F., Danyushevsky, L.V. and Chang, Z.S. (2007) Multistage Sedimentary and Metamorphic Origin of Pyrite and Gold in the Giant Sukhoi Log Deposit, Lena Gold Province, Russia. *Economic Geology*, **102**, 1232-1267. https://doi.org/10.2113/gsecongeo.102.7.1233

[17] Le Mignot, E., Reisberg, L. andré-Mayer, A.-S., Bourassa, Y., Fontaine, A. and Miller, J. (2017) Re-Os Geochronological Evidence for Multiple Paleoproterozoic Gold Events at the Scale of the West African Craton. *Economic Geology*, **112**, 145-168. https://doi.org/10.2113/econgeo.112.1.145

[18] Pons, J., Barbey, P., Dupuis, D. and Léger, J.M. (1995) Mechanisms of Pluton Emplacement and Structural Evolution of a 2.1 Ga Juvenile Continental Crust: The Birimian of Southwestern Niger. *Precambrian Research*, **70**, 281-301. https://doi.org/10.1016/0301-9268(94)00048-V

[19] Gasquet, D., Barbey, P., Adou, M. and Paquette, J.L. (2003) Structure Sr-Nd Isotope Geochemistry and Zircon U-Pb Geochronology of the Granitoids of the Dabakala Area (Côte d'Ivoire): Evidence for a 2.3 Ga Crustal Growth Event in the Paleoproterozoic of West Africa? *Precambrian Research*, **127**, 329-354. https://doi.org/10.1016/S0301-9268(03)00209-2

[20] Doumbia, S., Pouclet, A., Kouamelan, A., Peucat, J.J., Vidal, M. and Delor, C. (1998) Petrogenesis of Juvenile-Type Birimian (Paleoproterozoic) Granitoids in Central Cote-d'Ivoire, West Africa: Geochemistry and Geochronology. *Precambrian Research*, **87**, 33-63. https://doi.org/10.1016/S0301-9268(97)00201-5

[21] Naba, S., Lompo, M., Débat, P., Bouchez, J.L. and Béziat, D. (2004) Structure and Emplacement Model for Late-Orogenic Paleoproterozoic Granitoids: The Tenkodogo-Yamba Elongate Pluton (Eastern Burkina Faso). *Journal of African Earth Sciences*, **38**, 41-57. https://doi.org/10.1016/j.jafrearsci.2003.09.004

[22] Vegas, N., Naba, S., Bouchez, J.L. and Jessell, M. (2008) Structure and Emplacement of Granite Plutons in the Paleoproterozoic Crust of Eastern Burkina Faso: Rheological Implications. *International Journal of Earth Sciences*, **97**, 1165-1180. https://doi.org/10.1007/s00531-007-0205-z

[23] Metelka, V., Baratoux, L., Naba, S. and Jessell, M.W. (2011) A Geophysically Constrained Litho-Structural Analysis of the Eburnean Greenstone Belts and Associated Granitoid Domains, Burkina Faso, West Africa. *Precambrian Research*, **190**, 48-69. https://doi.org/10.1016/j.precamres.2011.08.002

[24] Leube, A., Hirdes, W., Mauer, R. and Kesse, G.O. (1990) The Early Proterozoic Birimian Super Group of Ghana and Some Aspects of Its Associated Gold Mineralization. *Precambrian Research*, **46**, 139-165. https://doi.org/10.1016/0301-9268(90)90070-7

[25] Hirdes, W., Davis, D.W., Ltidtke, G. and Konan, G. (1996) Two Generations of Birimian (Paleoproterozoic) Volcanic Belts in Northeastern Côte d'Ivoire (West Afri-

ca): Consequences for the "Birimian Controversy". *Precambrian Research*, **80**, 173. https://doi.org/10.1016/S0301-9268(96)00011-3

[26] Pouclet, A., Vidal, M., Delor, C., Simeon, Y. and Alric, G. (1996) Le volcanisme birimien du nord-est de la Côte-d'Ivoire, mise en évidence de deux phases volcanotectoniques distinctes dans l'évolution géodynamique du Paléoprotérozoïque. *Bulletin de la Société Géologique de France*, **167**, 529-541.

[27] Feybesse, J.L., Billa, M., Guerrot, C., Duguey, E., Lescuyer, J.L., Milési, J.P. and Bouchot, V. (2006) The Paleoproterozoic Ghanaian Province: Geodynamic Model and Ore Controls, Including Regional Stress Modeling. *Precambrian Research*, **149**, 149-196. https://doi.org/10.1016/j.precamres.2006.06.003

[28] Baratoux, L., Metelka, V., Naba, S., Ouiya, P., Siebenaller, L., Jessel, M., Salvi, S., Béziat, D. and Franceschi, G. (2015) Tectonic Evolution of the Gaouaregion, Burkina Faso: Implication for Mineralisation. *Journal of African Earth Sciences*, **112**, 419-439. https://doi.org/10.1016/j.jafrearsci.2015.10.004

[29] Ouiya, P., Siebenaller, L., Salvi, S., Béziat, D., Naba, S., Baratoux, L., Naré, A. and Franceschi, G. (2016) The Nassara Gold Prospect, Gaoua District, Southwestern Burkina Faso. *Ore Geology Reviews*, **78**, 623-630. https://doi.org/10.1016/j.oregeorev.2015.11.026

[30] Ouiya, P., Naba, S., Iiboudo, H., Sawadogo, S. and Yaméogo, A.O. (2020) Mise en évidence de structures principales et connexes contrôlant la minéralisation dans le district aurifère de Nassara au sud-ouest du Burkina Faso (Afrique de l'ouest). *Journal des sciences*, No. 1, 1-21.

[31] Winchester, J.A. and Floyd, P.A. (1977) Geochemical Discrimination of Different Magma Series and Their Differentiation Products Using Immobile Elements. *Chemical Geology*, **20**, 325-343. https://doi.org/10.1016/0009-2541(77)90057-2

[32] Jenen, L.S. (1976) A New Cation Plot for Classifying Sub-Alkaline Volcanic Rocks. Ontario Division Mines Miscellaneous Paper No. 66.

[33] Miyashiro, A. (1974) Volcanic Rock Series in Island Arcs and Active Continental Margins. *American Journal of Science*, **274**, 321-355. https://doi.org/10.2475/ajs.274.4.321

[34] McDonough, W.F. and Sun, S. (1995) The Composition of the Earth. *Chemical Geology*, **120**, 223-253. https://doi.org/10.1016/0009-2541(94)00140-4

[35] Storey, M., Mahoney, J.J., Kroenke, L.W. and Saunders, A.D. (1991) Are Oceanic Plateaus Sites of Komatiite Formation? *Geology*, **19**, 376-379. https://doi.org/10.1130/0091-7613(1991)019<0376:AOPSOK>2.3.CO;2

[36] Sun, S.S. and McDonough, W.F. (1989) Chemical and Isotopic Systematics of Oceanic Basalts: Implications for Mantle Composition and Processes. In: Sanders, A.D. and Norry, M.J., Eds., *Magmatism in the Ocean Basins*, Vol. 42, Geological Society Special Publication, London, 313-345. https://doi.org/10.1144/GSL.SP.1989.042.01.19

[37] Taylor, P.N., Moorbath, S., Leube, A. and Hirdes, W. (1992) Early Proterozoic Crustal Evolution in the Birimian of Ghana: Constraints from Geochronology and Isotope Geochemistry. *Precambrian Research*, **56**, 97-111. https://doi.org/10.1016/0301-9268(92)90086-4

[38] Pouclet, A., Doumbia, S. and Vidal, M. (2006) Geodynamic Setting of the Birimian Volcanism in Central Ivory Coast (Western Africa) and Its Place in the Palaeoproterozoic Evolution of the Man Shield. *Bulletin de la Societe Geologique de France*, **177**, 105-121. https://doi.org/10.2113/gssgfbull.177.2.105

[39] Hollings, P. and Kerrich, R. (2004) Geochemical Systematics of Tholeiites from 2.86

Ga Pickle Crow Assemblage, Northwestern Ontario: Arc Basalts with Positive and Negative Nb-Hf Anomalies. *Precambrian Research*, **134**, 1-20. https://doi.org/10.1016/j.precamres.2004.05.009

[40] Condie, K.C. (1999) Mafic Crustal Xenoliths and the Origin of the Lower Continental Crust. *Lithos*, **46**, 95-101. https://doi.org/10.1016/S0024-4937(98)00056-5

[41] Condie, K.C. (2003) Incompatible Element Ratios in Oceanic Basalts and Komatiites: Tracking Deep Mantle Sources and Continental Growth Rates with Time. *Geosystems*, **4**, 1-28. https://doi.org/10.1029/2002GC000333

[42] Condie, K.C. (2005) High Field Strength Element Ratios in Archean Basalts: A Window to Evolving Sources of Mantle Plumes? *Lithos*, **79**, 491-504. https://doi.org/10.1016/j.lithos.2004.09.014

[43] Sproule, R.A., Lesher, C.M., Ayer, J.A., Thurston, P.C. and Herzberg, C.T. (2002) Spatial and Temporal Variations in the Geochemistry of Komatiites and Komatiitic Basalts in the Abitibi Greenstone Belt. *Precambrian Research*, **115**, 153-186. https://doi.org/10.1016/S0301-9268(02)00009-8

[44] Kerrich, R., Polat, A., Wyman, D.A. and Hollings, P. (1999) Trace Element Systematics of Mg- to Fe-Tholeiitic Basalt Suites of the Superior Province: Implications for Archean Mantle Reservoirs and Greenstone Belt Genesis. *Lithos*, **46**, 163-187. https://doi.org/10.1016/S0024-4937(98)00059-0

[45] Goldfarb, R.J., Groves, D.I. and Gardoll, S. (2001) Orogenic Gold and Geologic Time: A Global Synthesis. *Ore Geology Reviews*, **18**, 1-75. https://doi.org/10.1016/S0169-1368(01)00016-6

[46] Groves, D.I., Goldfarb, R.J., Gebre-Mariam., M., Hagemann, S.G and Robert, F. (1998) Orogenic Gold Deposits: A Proposed Classification in the Contrast of Their Crustal Distribution and Relationship to Other Gold Deposit Types. *Ore Geology Reviews*, **13**, 7-27. https://doi.org/10.1016/S0169-1368(97)00012-7

[47] Groves, D.I., Goldfarb, R.J., Robert, F. and Hart, C.J.R. (2003) Gold Deposits in Metamorphic Belts: Overview of Current Understanding, Outstanding Problems, Future Research, and Exploration Significance. *Economic Geology*, **98**, 1-29. https://doi.org/10.2113/gsecongeo.98.1.1

[48] Groves, D.I., Condie, K.C., Goldfarb, R.J., Hronsky, J.M.M. and Vielreicher, R.M. (2005) Secular Changes in Gold Tectonic Processes and Their Influence on The Temporal Distribution of Gold-Bearing Mineral Deposits. *Economic Geology*, **100**, 203-224. https://doi.org/10.2113/gsecongeo.100.2.203

[49] Oppliger, G.L., Murphy, J.B. and Brimhall Jr., G.H. (1997) Is the Ancestral Yellowstone Hotspot Responsible for the Tertiary "Carlin" Mineralization in the Great Basin of Nevada? *Geology*, **25**, 627-630. https://doi.org/10.1130/0091-7613(1997)025<0627:ITAYHR>2.3.CO;2

[50] Bierlein, F.P., Stein, H.J., Coira, B. and Reynolds, P. (2006) Timing of Gold and Crustal Evolution of the Paleozoic South Central Andes, NW Argentina-Implications for the Endowment of Orogenic Belts. Earth Planet. *Science Letters*, **245**, 702-721. https://doi.org/10.1016/j.epsl.2006.03.019

[51] Goldfarb, R.J., Baker, T., Dubé, B., Groves, D.I., Hart, C.J.R. and Gosselin, P. (2005) Distribution, Character, and Genesis of Gold Deposits in Metamorphic Terranes. In: Hedenquist, J.W., *et al.*, Eds., *Economic Geology*: 100*th Anniversary Volume*, Society of Economic Geologists, McLean, 407-450. https://doi.org/10.5382/AV100.14

[52] Phillips, G.N., Groves, D.I. and Brown, I.J. (1987) Source Requirements for the Golden Mile, Kalgoorlie: Significance to the Metamorphic Replacement Model of

Archean Gold Deposits. *Canadian Journal of Earth Sciences*, **24**, 1643-1651. https://doi.org/10.1139/e87-158

[53] Traoré, Y.D., Siebenaller, L., Salvi, S., Béziat, D. and Bouaré, M.L. (2016) Progressive Gold Mineralization along the Syama Corridor, Southern Mali (West Africa). *Ore Geology Reviews*, **78**, 586-598. https://doi.org/10.1016/j.oregeorev.2015.11.003

Appendix. Supplementary Geochemical Analyses of Nassara Basalts

Representative major (wt%) and trace (ppm) element compositions for the Nassara basaltic rocks.

SAMPLE	Ba15	Ba16	Ba17	Ba18	Ba19	Ba20	Ba21	Ba22	Ba23	Ba24	Ba25	Ba26	Ba27	Ba28
Major elements (wt%)														
SiO_2	47.4	48.9	47.2	49	49.2	49	47	49.3	47.9	49.6	47.5	47	48.9	49
Al_2O_3	13.6	13.6	13.4	14	14.1	13	13	13.7	12.9	13.3	15.4	14	14.2	13
Fe_2O_3	14.1	14.5	14.5	14	16.2	15	15	16.1	15.3	15	12.6	13	14	15
CaO	9.48	11.1	11.9	11	8.91	9.44	4.9	8.94	9.06	10.2	11.9	11	9.87	9.3
MgO	7.04	6.87	6.63	6.9	5.93	6.17	4.6	5.84	6.13	5.8	5.22	6.6	6.49	5.9
Na_2O	2.63	2.29	1.92	2.1	3.07	2.4	2.9	2.86	2.49	2.6	1.8	1.8	2.85	2.6
K_2O	0.16	0.02	0.23	0.1	0.16	0.04	0	0.21	0.03	0.07	0.27	0.2	0.16	0.2
Cr_2O_3	0.05	0.06	0.06	0.1	0.03	0.05	0	0.03	0.04	0.04	0.05	0.1	0.05	0
TiO_2	0.98	1.12	1.12	1.1	1.24	1.19	1.2	1.25	1.21	1.2	0.88	0.9	0.91	1.2
MnO	0.21	0.22	0.2	0.2	0.21	0.22	0.2	0.21	0.22	0.22	0.19	0.2	0.2	0.2
P_2O_5	0.09	0.12	0.15	0.1	0.11	0.11	0.1	0.11	0.1	0.11	0.07	0.1	0.08	0.1
SrO	0.01	0.01	0.04	0	0.01	0.02	0	0.01	0.01	0.01	0.01	0	0.01	0
BaO	0.01	0.01	0.01	0	0.01	0.01	0	0.01	0.01	0.01	0.01	0	0.01	0
LOI	3.08	2.93	2.95	3.2	1.78	4.14	9.5	3.07	3.8	3.22	3.41	2.8	2.36	2.7
total	98.84	101	100.3	101.8	100.9	100.79	98.4	101.6	99.2	101.4	99.3	97.7	100.1	99.2
Traces elements (ppm)														
Ba	52.1	22.5	56.4	28	40.3	27.3	74	37.5	25.9	26.1	23.6	41	33.8	63
Ce	11.3	12	13.2	13	8.8	9.2	11	7.9	8.6	8.9	7	7.1	7.8	9.1
Cr	270	500	520	470	230	380	120	180	290	290	420	370	400	250
Cs	0.13	0.12	0.12	0.1	0.18	0.79	0.4	1.06	0.72	0.4	0.56	0.2	0.24	0.4
Dy	3.92	4.94	5.17	5.1	4.71	5.02	5.4	4.47	4.89	4.99	3.48	3.3	3.56	5
Er	2.6	3.35	3.59	3.3	3.07	3.53	3.6	3.03	3.31	3.47	2.45	2.3	2.52	3.4
Eu	0.97	0.95	1.11	1	1.01	1.02	1.1	0.91	0.97	1	0.77	0.7	0.81	1
Ga	15.4	16.3	18.2	17	17.7	17.7	17	15.8	18	18.4	16.6	16	16.3	18
Gd	3.33	3.7	4.12	3.8	3.82	4	4.4	3.37	3.72	3.9	2.73	2.8	2.9	3.9
Hf	1.9	2.1	2.2	2.1	2.1	2.1	2.3	1.6	2	2	1.7	1.5	1.5	1.8
Ho	0.86	1.02	1.18	1.1	1.04	1.11	1.2	0.97	1.04	1.08	0.76	0.7	0.81	1.1
La	4.5	4.6	5.3	4.9	3.2	3.4	4.5	2.9	3.2	3.3	2.5	2.6	2.9	3.4
Lu	0.42	0.53	0.54	0.5	0.48	0.52	0.6	0.46	0.51	0.52	0.38	0.4	0.4	0.5
Nb		4.9	5	5.1							2.1	2	2.2	
Nd	8.2	8.4	9.5	8.8	7.5	7.7	8.8	6.6	6.8	7.4	5.5	5.8	6	7.4
Pr	1.67	1.75	1.91	1.8	1.34	1.44	1.7	1.23	1.32	1.41	1.14	1.1	1.18	1.5
Rb	2	0.2	5.1	1.8	1.7	0.8	1.3	4	0.8	1.1	10.1	3.7	3.3	5.2

Continued

Sm	2.47	2.81	3.01	3	2.65	2.79	3	2.11	2.68	2.73	2.02	1.9	2	2.7
Sr	79.5	76.7	382	169	99.3	152	97	100	127	107	137	81	99.4	121
Tb	0.59	0.68	0.76	0.7	0.67	0.75	0.8	0.61	0.67	0.7	0.49	0.5	0.54	0.7
Th	0.39	0.37	0.43	0.4	0.28	0.29	0.4	0.29	0.27	0.28	0.18	0.2	0.28	0.3
Ti	0.5	0.5	0.5	0.5	0.5	0.50	0.5	0.5	0.5	0.5	0.5	0.5	0.5	0.5
Tm	0.4	0.51	0.53	0.5	0.46	0.54	0.6	0.44	0.51	0.48	0.36	0.4	0.37	0.5
U	0.12	0.1	0.14	0.1	0.09	0.08	0.1	0.08	0.09	0.09	0.05	0.1	0.09	0.1
V	364	280	315	285	397	424	406	359	405	405	336	342	353	401
Y	23.2	28.9	31.1	30	28.8	30.1	32	26	29.2	29.7	20.6	21	21.3	30
Yb	2.52	3.16	3.51	3.3	3.18	3.33	3.5	2.95	3.16	3.48	2.37	2.4	2.37	3.2
Zr	59	69	72	70	62	63	71	54	66	64	53	46	51	60
Cu	229	186	275	181	134	149	172	168	158	131	143	137	142	166
Ni	120	344	196	137	112	143	66	86	232	133	145	134	143	138
Zr/Y	2.54	2.38	2.31	2.33	2.15	2.09	2.21	2.07	2.26	2.15	2.57	2.19	2.39	2
Zr/Nb		14.08	14.4	13.72							25.23	23	23.18	
Nb/Th		13.24	11.62	12.75							11.66	10	7.85	
Nb/Y		0.16	0.16	0.17							0.10	0.09	0.10	
Eu/Eu*	1.03	0.90	0.96	0.90	0.97	0.93	0.92	1.04	0.94	0.94	1.00	0.93	1.03	0.94
(La/Yb)N	1.22	0.99	1.03	1.01	0.68	0.69	0.88	0.67	0.69	0.65	0.72	0.74	0.83	0.72
(La/Sm)N	1.14	1.03	1.10	1.02	0.76	0.76	0.94	0.86	0.75	0.76	0.78	0.86	0.91	0.79